PHYSICAL REVIEW E VOLUME 55, NUMBER 6 JUNE 1997

Reflection of nonlinear waves from a domain boundary

A. La Porta and C. M. Surko
Department of Physics, University of California, San Diego, La Jolla, California 92093
(Received 28 October 1996)

Boundaries between domains of traveling waves are studied in convection in an 8% mixture of ethanol and water. A configuration is described in which rolls move in opposite directions on either side of a domain wall. Demodulation techniques are used to measure the interaction of waves across the boundary. It is found that rolls approaching the boundary with an oblique angle of incidence are reflected from the boundary. The reflection coefficient and the attenuation of the reflected wave are measured. [S1063-651X(97)50106-1]

PACS number(s): 47.54.+r, 47.27.Te, 47.20.Ky

When a spatially extended system is driven far from equilibrium, a homogeneous initial state may become unstable to a spatial modulation. The subsequent formation of a pattern can fundamentally change the physical properties of the system, such as mass or energy transport. Examples are as diverse as the excitation of transverse spatial modes in a large aperture laser, the formation of chemical waves in a reaction-diffusion system, and the formation of convection rolls in a fluid layer heated from below. Such nonequilibrium systems are not constrained by a free-energy minimization principle and very complicated pattern dynamics can occur [1].

The great richness of the dynamics of nonequilibrium patterns is particularly evident in systems that have an oscillatory instability. Patterns in such systems generally consist of traveling waves or superpositions of traveling waves. In two dimensions, oscillatory patterns can take many forms, including spiral waves, target waves, disordered superpositions of waves, and multiple domains of traveling waves. In this last case, the properties of the boundaries between traveling-wave domains are central to the dynamics of the patterns and have been studied extensively in analytical models [2–4].

In this Rapid Communication, we describe an investigation of two-dimensional (2D) traveling-wave convection patterns in a mixture of ethanol and water. The patterns are found to consist of domains of nonlinear traveling waves separated by stable domain boundaries [5]. We employ 3D complex demodulation techniques to characterize the interaction of waves at the boundary for a specific configuration, known as a ''zipper.'' We report a strong exclusion of waves from neighboring domains and present evidence that waves incident on a domain boundary are reflected as if the boundary were a rigid obstacle. This suggests that in this strongly nonlinear wave system, a domain of counterpropagating waves is equivalent to an impenetrable medium.

Rayleigh-Bénard convection in a binary mixture of ethanol and water is a widely studied example of a nonequilibrium system whose primary instability is oscillatory. In this system, a thin fluid layer is heated from below and the thermal expansion of the fluid tends to create an unstable density profile which can drive a convective flow. The forcing parameter is the Rayleigh number, Ra, which is a dimensionless measure of the temperature difference imposed across the fluid layer. In ethanol-water mixtures, there is a large Soret effect, so that the transport of ethanol in the mixture is driven by a temperature gradient. As a result, when a temperature difference is applied across the fluid layer, an ethanol concentration gradient develops, which also contributes to the fluid density profile. The ratio of concentration buoyancy to thermal buoyancy is given by the separation ratio ψ [1]. The system is also characterized by the Prandtl number, Pr, which is the ratio of thermal diffusivity to viscosity, and the Lewis number, $\mathcal{L}$, which is the ratio of thermal diffusivity to solute diffusivity [1].

The fluid used in the experiment is a mixture of 8% ethanol (by weight) in water at a mean temperature of 26 °C, for which $\psi=-0.24$, Pr=10.5, and $\mathcal{L}\approx 10^{-2}$ [6]. For this large negative value of ψ and strong separation of the time scales of thermal and mass diffusion, the onset of convection is a strongly subcritical Hopf bifurcation to a state of oscillating convection, which subsequently increases in amplitude until continuously overturning traveling-wave convection is triggered. Superpositions of waves are typically observed in the small-amplitude oscillatory state and the flow in this regime takes the form of weakly nonlinear waves [7]. After the formation of the large-amplitude traveling-wave state, the wave components interact strongly and the dominant wave component in a region of the pattern quickly suppresses the other wave components. This causes the initially disordered pattern to partition itself into domains of traveling waves, separated by well-defined domain walls [5]. In this case, the interaction of wave components occurs mainly at these domain walls, where a narrow region remains in which the waves overlap.

The experiments were performed in a cylindrical convection cell having an aspect ratio (r/h) of 26. The pattern is visualized by a white-light shadowgraph and video sequences are recorded using a charge-coupled-device camera and a frame grabber. Below, distances are expressed in terms of the cell height, $h=0.4$ cm, and times are expressed in terms of the vertical thermal diffusion time, $\tau=124$ s. A detailed description of the apparatus and of the physical parameters of the experiment have been published elsewhere [5].

Figure 1 shows a snapshot of an area of a traveling-wave convection pattern observed at $r=1.35$, containing a domain boundary. This boundary is known as a zipper and is one of several types of domain boundaries observed in traveling-wave (TW) convection patterns [8,5]. In a zipper, rolls on either side of the boundary move in roughly opposite directions, in a configuration reminiscent of a shear flow. As the

 © 1997 The American Physical Society

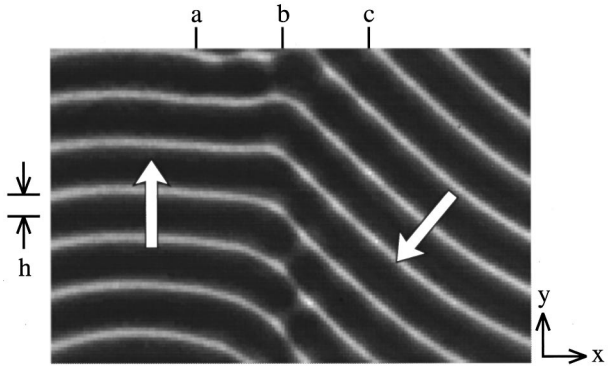

FIG. 1. A shadowgraph image of a region of a convection pattern containing a zipper boundary. The arrows indicate the direction of propagation within each domain.

rolls move past each other, there is a repeated disconnection and reconnection of the convection rolls across the boundary. The kinematics of the boundary can be appreciated by examining space-time plots of the pattern, which are shown in Fig. 2. Figure 2(a) shows a y-t plot taken at the position marked a in Fig. 1. The diagonal stripes indicate propagation in the positive y direction and the phase velocity is given by the inverse slope of the stripes. Similarly, Fig. 2(c) shows a y-t plot at a position on the other side of the boundary, marked c in Fig. 1, and indicates propagation in the negative y direction. The pattern in Fig. 2(b) was recorded at position b, at the center of the domain boundary, where disconnection and reconnection of rolls occur. This is a standing-wave pattern, indicating that the domain boundary consists of a region of overlap of the two wave components.

One method of characterizing superpositions of wave components is to perform a spatiotemporal demodulation of the pattern [9]. We assume that the pattern consists of a superposition of several wave components that are modulated by slowly varying envelopes. Then, the pattern $A(x,t)$ can be expressed in the form,

$$A(\mathbf{x},t)=\mathrm{Re}[A_1(\mathbf{x},t)\exp(\mathbf{k}_1\cdot\mathbf{x}-\omega t) + A_2(\mathbf{x},t)\exp(\mathbf{k}_2\cdot\mathbf{x}-\omega t)+\cdots], \quad (1)$$

where the $\mathbf{k}_n$ are the dominant wave vector components in the data and the $A_n(\mathbf{x},t)$ are the unknown complex amplitudes of the spatiotemporal waves. These amplitudes can be calculated as follows. The data are multiplied by a spatiotemporal carrier chosen to match one of the wave components, $\exp(\mathbf{k}_n\cdot\mathbf{x}-\omega t)$. This produces components at sum and difference frequencies between the carrier wave and the data so that the selected wave component in the data is mapped to zero frequency. Then, all other components can be eliminated by applying a low-pass spatiotemporal filter. The resulting amplitude is the envelope function, $A_n(\mathbf{x},t)$.

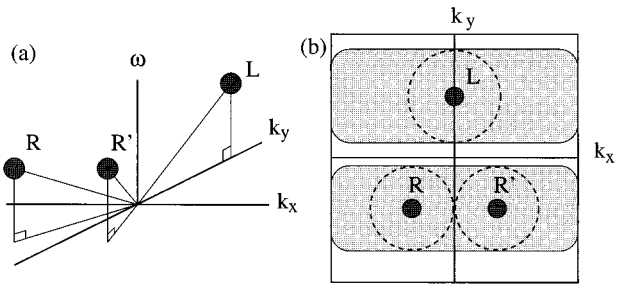

FIG. 3. (a) A schematic representation of the 3D spatiotemporal Fourier transform of the domain boundary in Fig. 1. (b) The projection of the Fourier transform on the k_x-k_y plane. The spots marked L and R are due to rolls passing on the left and right of the domain boundary, respectively, and the spot marked R' indicates rolls reflected from the right of the boundary. The shaded rectangles and dotted circles in (b) represent filters applied to the spectrum and are discussed in the text.

A schematic representation of the spatiotemporal Fourier transform of the pattern in Fig. 1 is shown in Fig. 3. The two domains in the pattern produce distinct spectral components, labeled L, which lies near the k_y axis at $\mathbf{k}_L=(-0.18,3.20)$, and R, which lies at $\mathbf{k}_R=(2.19,-2.47)$, where the subscripts L and R refer to rolls to the left and right of the boundary. These wave vectors, along with the temporal frequency of $\omega=0.14\tau^{-1}$, are taken as the spatiotemporal carrier waves. Our main purpose is to evaluate the dependence of $A_n(\mathbf{x},t)$ on the coordinate transverse to the domain boundary. The low-pass spatial filter is therefore chosen to depend only on $\mathbf{k}_y$. The shaded rectangles in Fig. 3 indicate the band of spatial frequencies passed by the spatial filter. This filter is sufficient to separate the two main frequency components, and gives maximum resolution of $A(\mathbf{x},t)$ in the x direction.

The demodulated amplitudes for the two wave vectors, $\mathbf{k}_L$ and $\mathbf{k}_R$ are shown in Fig. 4. The amplitude fields, $A_L(\mathbf{x},t_0)$ and $A_R(\mathbf{x},t_0)$, are represented as elevation surfaces over the shadowgraph image. The abrupt crossover from one component to the other is evident, as well as some interesting structure in the amplitude fields in the vicinity of the domain boundary. Figure 5(a) shows the amplitudes as a function of x for y fixed at the midpoint of the domain boundary. From the line plots, it can be determined that the amplitude goes from its nominal value of unity to zero in a distance of approximately $0.83d$, where d is the cell height (i.e., 0.415λ, where λ is the roll wavelength). This abrupt cutoff indicates the strong suppression of counterpropagating waves within a

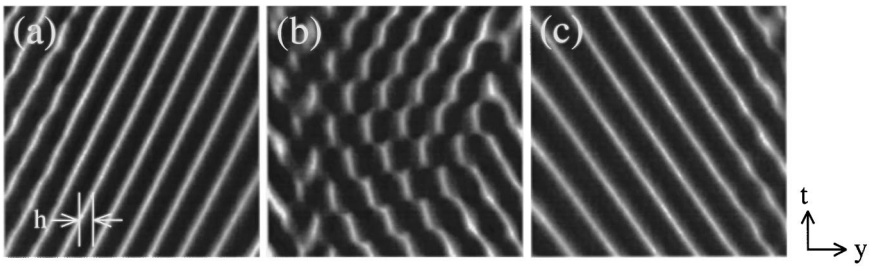

FIG. 2. Space-time plots taken along several lines parallel to the domain boundary. These plots are taken from 128 video frames, spanning 31τ. The positions of the lines relative to the boundary are indicated by the labels at the top of Fig. 1.

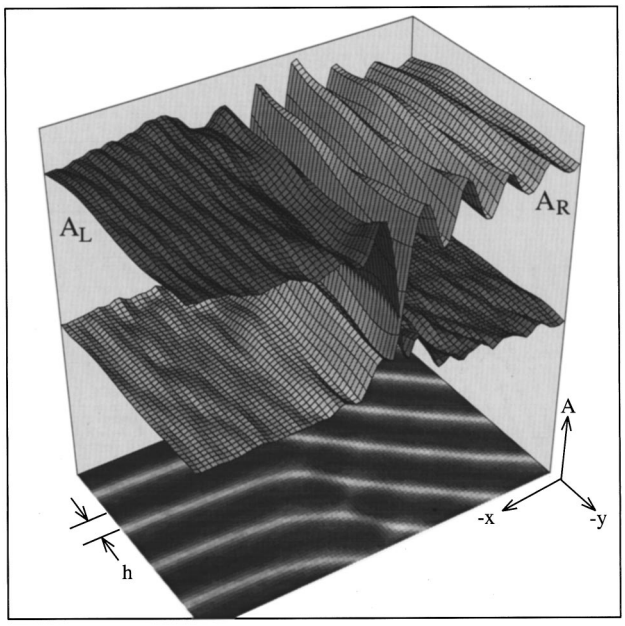

FIG. 4. Elevation plot of the amplitudes calculated for wave vectors $\mathbf{k}_L$ and $\mathbf{k}_R$. The interpenetrating dark gray and light gray surfaces represent $A_L(\mathbf{x},t_0)$ and $A_R(\mathbf{x},t_0)$, respectively, and the plane at the bottom shows the corresponding area of the convection pattern.

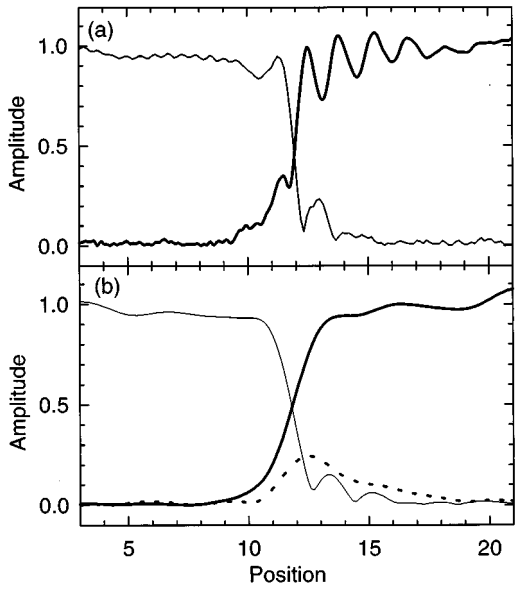

FIG. 5. The amplitudes $A_L(\mathbf{x},t_0)$ (fine line), $A_R(\mathbf{x},t_0)$ (bold line), and $A_{R'}(\mathbf{x},t_0)$ (dotted line) as a function of x at a constant y_0, at the midpoint of the domain boundary. The amplitudes are shown (a) with k_y filtering and (b) with $\|k\|$ filtering, as described in the text.

domain of traveling waves and is in qualitative agreement with the analytic model of Aranson and Tsimring [3].

Another interesting feature of the amplitudes is that $A_L(\mathbf{x},t_0)$, which represents rolls moving along the boundary, is quite flat, except for a sharp lip near the boundary, whereas $A_R(\mathbf{x},t_0)$, exhibits a prominent modulation in the x direction that decays as a function of the distance from the boundary. This modulation is evidence of a standing wave, arising from the interference between the wave at $\mathbf{k}_R$ and another wave with a different value of k_x (but with the same value of k_y, since there is no modulation of the amplitude in the y direction). The wave number of the standing wave in $A_R(\mathbf{x},t_0)$, which indicates the difference in k_x between the two wave components, is $k_s=4.4\pm0.1$. Noting that within experimental error $k_s=2(\mathbf{k}_R)_x$, this standing-wave pattern is consistent with the geometrical reflection of the waves $\mathbf{k}_R$ from the domain boundary, for which $k_x\rightarrow-k_x$ and $k_y\rightarrow k_y$. No evidence of a reflected wave is observed in $A_L(\mathbf{x},t_0)$ and none is expected, since $\mathbf{k}_L$ has no significant component normal to the boundary.

The function $A_R(\mathbf{x},t)$ exhibits a standing wave because the spatial filter used in the demodulation admits both the incident and reflected wave vectors. In order to separate the incident and reflected waves, the demodulation was repeated with isotropic filtering about the carrier wave vectors, as indicated by the dotted circles in Fig. 3(b). In Fig. 5(b), the amplitudes are shown for the primary wave vectors, $\mathbf{k}_L$ and $\mathbf{k}_R$, as well as for the reflected wave vector, $\mathbf{k}_{R'}$. In these curves, the abrupt cutoff at the boundary is softened by the transverse filtering and the standing-wave pattern previously seen in $A_R(\mathbf{x},t_0)$ is gone. However, the reflected wave, whose amplitude is indicated by the dotted curve, is clearly resolved. The amplitude of the reflected wave at the interface is about 0.25 of the amplitude of the incident wave and appears to decay exponentially with x at a rate $\alpha=0.37d^{-1}$. This decay of the minority wave component is presumably related to the instability of superpositions of wave components in this system.

The reflected wave can also be isolated by applying a spatiotemporal filter to the video record of the pattern. The three panels in Fig. 6 show the pattern data after the application of spatiotemporal band-pass filters centered on $\mathbf{k}_L$, $\mathbf{k}_R$, and $\mathbf{k}_{R'}$.

In Table I, we summarize measurements on four zipper boundaries. In all cases, when the rolls approach the boundary at an oblique angle of incidence, a reflected wave is detected. There is no dependence of the reflected wave vector on the wave vector of the rolls on the opposite side of the boundary. The amplitude of the reflected wave seems to be greatest for an angle of incidence close to $\pi/4$, for which the incident and reflected rolls are perpendicular. This may be related to the tendency of cross-roll patterns to form in TW convection [5].

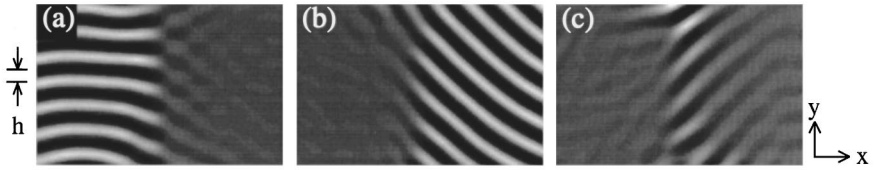

FIG. 6. Separated wave components from the data in Fig. 1. Panels (a), (b), and (c) show the wave components after application of spatiotemporal band-pass filters corresponding to the dotted circles surrounding L, R, and R' in Fig. 3.

TABLE I. Values of the transverse wave number, standing-wave wave number, and reflected component amplitude for all zippers studied. In all cases $\|\mathbf{k}_L\| \approx \pi$ and $\|\mathbf{k}_R\| \approx \pi$.

$(\mathbf{k}_L)_x$	$(\mathbf{k}_R)_x$	k_{Ls}	k_{Rs}	A_L	A_R
0.18	−2.19		4.5	0.00	0.25
2.10	1.46	4.05		0.20	0.00
2.15	0.99	4.30		0.18	0.00
1.61	0.09	3.40		0.08	0.00

To summarize, we have studied zipper domain boundaries in 2D traveling-wave convection patterns, and we have found them to be stable. In cases where rolls approach the boundary with an oblique incidence, we have found that a reflected wave is present. This result is unexpected. In weakly nonlinear systems, in which the nonlinear wave coupling is a perturbation on the linear wave propagation, a product wave can be generated by nonlinear wave mixing in regions where several waves overlap. The reflected wave vector is not consistent with such a process, which normally produces a phase conjugate wave. In TW convection, by contrast, the strong nonlinearity destabilizes superpositions of waves, causing traveling waves to be excluded from neighboring domains of counterpropagating waves. Therefore, the neighboring domain appears to be equivalent to an impenetrable medium. It is known that small-amplitude TW convection rolls can be reflected when incident on the system boundary [7,10,11] or on a domain of large-amplitude stationary rolls [12], and our data indicates that a similar reflection can occur when large-amplitude traveling rolls are incident on a counterpropagating domain of rolls.

We would like to acknowledge useful discussions with Paul Kolodner and Lev Tsimring. This work was supported by the U.S. Department of Energy under Grant No. DE-FG03-90ER14148.

[1] M. C. Cross and P. C. Hohenberg, Rev. Mod. Phys. **65**, 851 (1993).
[2] B. A. Malomed, Phys. Rev. E **50**, R3310 (1994).
[3] I. Aranson and L. Tsimring, Phys. Rev. Lett. **75**, 3273 (1995).
[4] P. Coullet, C. Elphick, L. Gil, and J. Lega, Phys. Rev. Lett. **59**, 884 (1987).
[5] A. La Porta and C. M. Surko, Phys. Rev. E **53**, 5916 (1996); Phys. Rev. Lett. **77**, 2678 (1996).
[6] P. Kolodner, H. Williams, and C. Moe, J. Chem. Phys. **88**, 6512 (1988).
[7] P. Kolodner, C. M. Surko, A. Passner, and H. L. Williams, Phys. Rev. A **36**, 2499 (1987).
[8] R. W. Walden, P. Kolodner, A. Passner, and C. M. Surko, Phys. Rev. Lett. **55**, 496 (1985).
[9] P. Kolodner, C. M. Surko, and H. Williams, Physica D **37**, 319 (1989).
[10] M. S. Bourzutschky and M. C. Cross, Phys. Rev. A **45**, 8317 (1992).
[11] E. Kaplan and V. Steinberg, Phys. Rev. E **48**, R661 (1993).
[12] P. Kolodner, Phys. Rev. E **48**, R665 (1993).